JOURNAL OF Materials CHEMISTRY

Synthesis and characterization of stable aqueous dispersions of silver nanoparticles through the Tollens process†

Yadong Yin,[a] Zhi-Yuan Li,[b] Ziyi Zhong,[b] Byron Gates,[b] Younan Xia*[b] and Sagar Venkateswaran[c]

[a]*Department of Materials Science and Engineering, University of Washington, Seattle, WA 98195, USA*
[b]*Department of Chemistry, University of Washington, Seattle, WA 98195, USA*
[c]*Peacock Laboratories, Inc., 54th Street and Paschall Ave., Philadelphia, PA 19143, USA*

Received 17th August 2001, Accepted 15th November 2001
First published as an Advance Article on the web 18th January 2002

This paper describes a simple and convenient procedure based on the Tollens process for the preparation of silver nanoparticles with a relatively narrow distribution in size. The starting reagents were similar to those commonly used in the electroless deposition of silver. Only under appropriate conditions, mixing of these reagents was able to generate stable aqueous dispersions of silver colloids rather than thin films of silver deposited on the surfaces of objects immersed in the plating solution (including the interior surface of the container). We have demonstrated the capability and feasibility of this approach by forming silver nanoparticles with dimensions in the range of 20–50 nm. These silver nanoparticles could exist as very stable dispersions in water, or as submonolayer coating on microscale colloids. We have also explored the use of light scattering simulation to study the oxidation (by air) of these nanoparticles.

I. Introduction

Metal nanoparticles have been extensively investigated because of their unique electronic and optical properties that are substantially different from bulk materials.[1] A lot of effort has been, in particular, devoted to the synthesis and characterization of stable dispersions of nanoparticles made of silver, gold, and other noble metals.[2] Part of the reason lies in the fact that these colloidal particles are useful in a broad range of areas, such as photography,[3] catalysis,[4] biological labeling,[5] photonics,[6] optoelectronics,[7] and surface-enhanced Raman scattering (SERS) detection.[8] A number of methods have been demonstrated in the past decades for preparing these nanoparticles; notable examples include condensation in the vapor phase,[9] chemical reduction in the solution phase,[10] photon- or ultrasound-induced reduction in solutions or reverse micelles,[11] chemical vapor deposition (CVD) or electrostatic spraying on solid substrates,[12] and thermal decomposition of precursors in solvents, sol–gel matrixes, and polymer films.[13] The dispersions of these nanoparticles usually display a very intense color due to plasmon resonance absorption, which can be attributed to the collective oscillation of conduction electrons that is induced by an electromagnetic field.[14] It has been shown that the size, morphology, stability, and properties (chemical or physical) of these nanoparticles have a strong dependence on the specificity of the preparation method and the experimental conditions.[15]

A rich variety of recipes are now available for producing silver nanoparticles as stable, colloidal dispersions in water or organic solvents.[16] It was generally accepted that preparation of discrete silver nanoparticles with well-defined shape and well-controlled dimensions was more difficult than that of gold nanoparticles due to the higher reactivity of silver compounds. We have recently reexamined the potential of the Tollens process in preparing silver nanoparticles. The main reaction involved in this process has been long employed in the electroless deposition of silver to generate reflective mirrors on solid supports.[17] These silvering solutions can be easily prepared by following the recipes outlined in a book written for amateur telescope makers.[17] They can also be obtained through a number of commercial sources.[18] The fundamental reaction involved in the Tollens process can be simplified as the following:

$$Ag(NH_3)_2^+(aq) + RCHO(aq) \rightarrow Ag(s) + RCOOH(aq) \quad (1)$$

Both aldehydes and reducing sugars can be employed for this process. The major difference between the present work and previous studies is that our protocol based on the Tollens process could provide a delay time of more than 5 min before the reaction occurred. This delay ensured a complete mixing of reactants, and the possibility of following the reaction using the UV–visible absorption spectroscopic technique. Such a relatively long period of initiation for the formation of silver nanoparticles also made it possible to achieve a good control over the particle size distribution. Without adding any stabilizing reagent, the as-synthesized aqueous dispersions of silver nanoparticles were found to be stable for at least one year.

II. Experimental

Materials

One can follow a number of recipes to prepare the so-called Tollens reagents—a set of solutions that are commonly exploited to electrolessly deposit thin films of silver to be used as mirrors or telescope coatings.[17] In this work, we have selected a commercial kit (HE-300) that is marketed by Peacock Laboratories, Inc. (Philadelphia, PA).[18] Each silvering kit comes as three separate aqueous solutions: (*A*) silver solution (silver nitrate); (*B*) activator solution (sodium hydroxide); and (*C*) reducer solution (formaldehyde and sorbitol). The silver solution contains 24–30% (by weight)

†Electronic supplementary information (ESI) available: photographs of silver mirror, and of stable dispersions of silver nanoparticles from mixing diluted silvering solutions under sonication at various times. See http://www.rsc.org/suppdata/jm/b1/b107469e/

 DOI: 10.1039/b107469e

silver nitrate and 28–34% ammonium hydroxide. The activator solution contains 7–12% sodium hydroxide and 6–10% ammonium hydroxide. The reducer solution contains 0.3% formaldehyde and 27–33% sorbitol. The silver ions in solution *A* will become reducible by solution *C*, only after they have been activated by adding solution *B*.

Preparation of silver nanoparticles

A typical procedure is shown as the following: (*i*) a mixture of solutions *A* and *B* was prepared by measuring 0.5 mL of the concentrated silver solution *A* into 14 mL deionized water, followed by the addition of 0.5 mL of the concentrated activator solution *B*. *Caution: to avoid the formation of explosive silver azide, do not mix concentrated silver solution with concentrated activator solution*. This solution was further diluted to 300 mL and referred to as "*SAB*". (*ii*) 0.5 mL of the concentrated reducer solution *C* was measured into a separate container and diluted to 300 mL with deionized water, and this solution was referred to as "*SC*". (*iii*) 0.9 mL of the *SAB* solution and the *SC* solution were mixed with 10 mL of water in a vial that was immersed in a sonication bath. Silver nanoparticles usually appeared in the solution after several minutes to half an hour. The length of this period depends on the reaction conditions such as concentrations of the reagents, reaction atmosphere (air *versus* nitrogen), ratio between different components, and temperature of the sonication bath. The reaction rate increased with increasing concentrations of reagents.

In all experiments, the reactions were carried out in a sonication bath (Branson 1210, Danbury, CT). These reactions could be completed within $\sim$30 min after the first appearance of light brown color. These aqueous dispersions of silver nanoparticles were also very stable and no sedimentation formed even after being stored for a period of one year.

Instrumentation

UV–Visible spectra were recorded with a 1 cm path length quartz cell using an HP 8453 spectrophotometer. Deionized water was used as the reference sample to take the "blank' spectrum for all measurements. TEM measurements were conducted on a JEM-1200 EX II electron microscope (JEOL, Peabody, MA) with an accelerating voltage of 80 kV. TEM samples were prepared by placing a drop of the colloidal dispersion on a copper grid (Ted Pella, coated with amorphous carbon). The samples involving intermediate products were quenched with dry ice immediately after the solutions were taken out of the reaction vessel and placed on TEM grids.

III. Results and discussions

Evolution of silver nanoparticles

The Tollens process has been used for many decades in the electroless deposition of silver mirrors by forming a thin film of silver on the surface of an object. When the activated silver solution *SAB* was directly mixed with the reducer solution *SC* in a glass vial, a shiny mirror formed on the inside of the vial within a few minutes. The solution contained some black precipitates which were characterized as aggregates of micro-scale silver particles with irregular morphologies. However, stable dispersions of silver nanoparticles, rather than thin films, could be obtained under sonication when the concentrations of reactants were reduced as described in the experimental section. For a wide range of reaction conditions, the solution went from clear and colorless at the time of mixing, through light brown, brown, to yellow-green. The final products were transparent dispersions of silver colloids with a bright yellow tint. As an advantage of the present method, the appearance of the first color change did not occur until all the reagents had been mixed and sonicated for a relatively long period of time (usually, several minutes to half an hour). All reactants can, therefore, be thoroughly mixed before reacting with each other. As a result, one can ensure that the reaction began and proceeded in a homogeneous and well-characterized environment, and the final product (silver nanoparticles) had a relatively narrow distribution in size. We believe the yellow-green stage involves a mixture of both brown and bright yellow. The transition from brown to bright yellow was relatively fast: usually within 1–2 min. Zukoski *et al.* also reported a similar color transition for their studies on the formation mechanism and aggregation behavior of silver nanoparticles prepared by reducing a silver perchlorate solution with borohydride.[19] Unfortunately, the initial reaction of their system was so fast (less than 0.5 s) that they were unable to unambiguously resolve the transition from colorless to brown. Because the reactants were not completely mixed, they also had difficulties in obtaining reproducible results.

We note that ultrasound has been successfully used by a number of research groups to initiate new reactions or to synthesize novel materials.[20] As the ultrasonic sound waves radiate through a solution, they may cause alternating high and low pressures in the solution. During the low-pressure stage, millions of microscopic bubbles can nucleate and grow. This process is called acoustic cavitation. During the high-pressure process, these bubbles collapse, or "implode', releasing enormous amounts of energy. As a result, extremely high temperatures and pressures are generated at the center of the collapsed bubbles. These conditions often lead to enhanced chemical reactivities. Although the intensity of the ultrasound we used in the present work is not very strong, we found that it might also have some accelerating effects on the formation of silver nanoparticles. The reaction performed under magnetic stirring was much slower than that carried out under sonication. In addition, the yield of the product under magnetic stirring was much lower as compared to the reactions initiated using sonication. Both of these observations were consistent with the fact that cavitation could greatly increase the nucleation rate by providing nucleation sites and forming a large number of seeds by breaking down the aggregates. Once the reaction had been initiated (with the appearance of a light brown color), the reaction vessel could be taken out from the sonication bath for continued growth of silver nanoparticles. The sonication may also have the effect of homogenizing the solution and maintaining a more uniform concentration profile than is possible with mechanical stirring. Therefore, a steady growth of the silver nanoparticles within this environment could produce relatively monodisperse samples.

In situ studies of the reaction

The homogeneity in the initial mixture of reactants also made it possible to follow the formation and evolution of silver nanoparticles *in situ* through UV–Vis absorption spectroscopy and transmission electron microscopy (TEM) methods. Fig. 1 shows some typical UV–Vis spectra of the solution after the reactants had been mixed and sonicated under an atmosphere of air for different periods of time at 27 °C. In this case, the color of the solution started to change from colorless to light brown after the reaction had proceeded for $\sim$15 min. This change in color suggests the formation of silver nanoparticles in the solution. Fig. 2A gives a TEM image of the sample taken from the solution at this stage. This TEM image indicates that only a very small amount of silver nanoparticles had formed up to this point, and the system seemed to be relatively unstable because the quasi-spherical particles exhibited a heterogeneous distribution in size. As the reaction proceeded (15–27 min), the brown color intensified, and the absorption also increased slightly at all wavelengths. The appearance of a brown color is largely due to the absorption in the long wavelength range

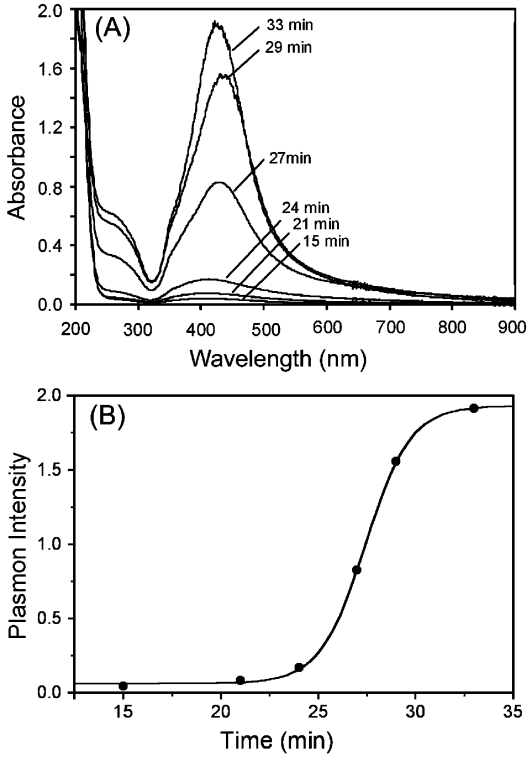

Fig. 1 (A) The UV–Vis absorption spectra taken from a reaction solution after the reactants had been mixed and sonicated in air at 27 °C for different periods of time. (B) A plot of the intensity of the plasmon peak against reaction time.

(500–800 nm). A typical TEM image of the silver particles formed during this period is shown in Fig. 2B. Compared with Fig. 2A, it is clear that most of the silver particles had significantly increased in size and the morphology had changed from quasi-spherical to highly irregular shapes. At this stage, the silver nanoparticles largely existed as aggregates. Some small particles (<10 nm) could still be observed in this sample, which were probably formed *via* a second round of nucleation. After the reaction had proceeded for $\sim$29 min, the intensity of the brown color reached its maximum. Although a few particles still remained as aggregates, most of them were discrete units exhibiting distinctive crystalline facets. As the reaction proceeded further, the intensity of the surface plasmon peak at $\sim$410 nm increased again while the absorption at wavelengths longer than 600 nm was essentially unchanged. At this point, a green color formed in the solution, giving the solution a yellow-green appearance. After the reaction had proceeded for $\sim$33 min, the solution exhibited a bright, transparent yellow coloration, which was stable with time. The intensity of the surface plasmon peak increased to its maximum value, and this value remained constant for at least 4–5 months. This sharp plasmon peak (with a full width at half maximum of $\sim$80 nm) indicates a very narrow distribution in the particle size. We also noted that the absorbance at wavelengths longer than 450 nm decreased slightly between 29 and 33 min, indicating a reduction in the particle size (probably from aggregates to discrete particles) in the solution. Again, our TEM observation is consistent with the UV–Vis spectroscopic measurements. As illustrated in Fig. 2C, the final product mainly consisted of individual nanoparticles of silver. Almost no aggregates of silver nanoparticles were observed.

In comparison with the TEM images reported by Heard *et al.*,[21] we could conclude that the silver nanoparticles synthesized using the present approach were a mixture of strongly faceted "multiple twinned particles' (MTPs, the majority) and single crystalline particles with triangular projection (as indicated by an arrow in Fig. 2C). The inset of

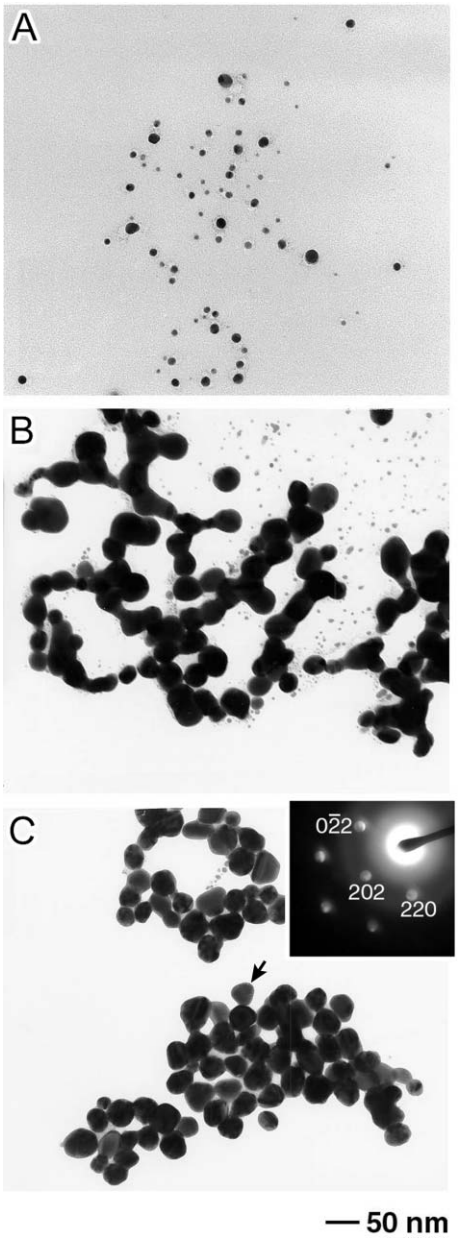

Fig. 2 The TEM images of silver nanoparticles that were sampled from the reaction solution shown in Fig. 1 after the reagents had been mixed and sonicated at 27 °C for (A) 15, (B) 27, and (C) 33 min, respectively. Silver nanoparticles with a broad distribution in size started to form at 15 min, and aggregated into irregular structures thereafter. Silver nanoparticles with distinctive crystalline facets were obtained after the reaction had proceeded for $\sim$33 min. The inset shows the electron microdiffraction pattern of a single crystalline silver nanoparticle (as indicated by an arrow).

Fig. 2C gives an electron microdiffraction pattern of the single crystalline silver nanoparticle. Analyzing the diffraction pattern suggested an fcc crystal structure with a lattice constant of $a = 4.073$ Å, which was in good agreement with the reported data ($a = 4.086$ Å, Joint Committee on Powder Diffraction Studies File No. 4-0783). Based on the data shown in Fig. 1 and 2, we could also conclude that the silver nanoparticles went through a decrease in size by more than one order of magnitude during the course of reaction. A similar observation for the formation of silver or gold nanoparticles using other chemical methods was also reported in literature.[9,22] According to their proposed mechanism, the nanoparticles were formed first in the solution and subsequently aggregated into large particles due to the electrostatic attraction. At the end of reaction, a change in the electrostatic condition led to a breakdown (similar to the Ostwald ripening

of a liquid jet) and redispersion of the nanoparticles as discrete objects. Fig. 1B gives a plot of the intensity of plasmon peak against reaction time. It clearly indicates a threshold time of ~15 min, within which essentially no silver nuclei were formed. In this case, the intensity of the plasmon peak reached a plateau after the reaction has proceeded for ~33 min, indicating the formation of a stable aqueous dispersion of silver nanoparticles.

Dependence of the reaction on temperature

We found that the formation and growth of silver nanoparticles was very sensitive to the temperature of the sonication bath. It took less time for the reaction to start and finish when the temperature was increased. This observation was in good agreement with the classical chemical kinetics. Fig. 3 shows TEM images of silver nanoparticles prepared under nitrogen at three slightly different temperatures: 27, 30 and 35 °C. The color of the reaction solution started to change at ~15, ~10, ~5.5 min, respectively. Although all these products were mixtures of discrete single crystalline and twinned particles exhibiting a similar morphology, the particle size changed from ~20, to ~30 and ~40 nm when the temperature was raised. We believe that the frequency of collision between the small particles increased as the temperature was raised, and thus led to the formation of larger particles. In their studies of silver nanoparticles grown *via* aggregation mechanism, Zukoski *et al.* also found that the growth rate of silver nanoparticle increased significantly with increasing reaction temperature.[23] They explained the temperature dependence of the particle size by pointing out that at the end of the intermediate stage the surface potential of silver particles decreased as the reaction temperature increased. At low temperatures, the aggregation rate was low because of a strong electrostatic repulsion (as caused by the high surface potential of the particles). As the temperature was increased, the surface potential dropped and resulted in a weaker repulsion and thus a higher growth rate. Based on this argument, small particles could only be stabilized at relatively low temperatures.

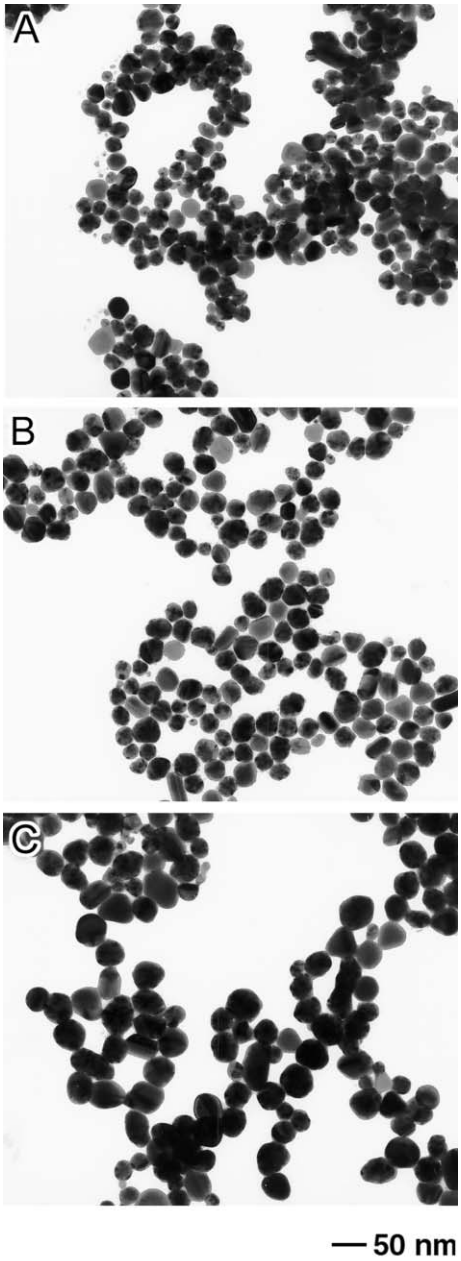

Fig. 3 The TEM images of silver nanoparticles that were obtained as the final products when the reactions were carried out under nitrogen at (A) 27, (B) 30, and (C) 35 °C, respectively. The mean size of these silver nanoparticles changed from ~20, to ~30 and ~40 nm when the temperature was raised.

Dependence of the reaction on atmosphere

We also found that the light scattering spectra of silver nanoparticles were highly sensitive to the reaction atmosphere. Fig. 4 shows the UV–Vis absorption spectra taken from three dispersions of silver nanoparticles prepared in different environments: with nitrogen bubbling, under an atmosphere of air without bubbling, and with bubbling of air. The surface plasmon peaks red-shifted (with a significant reduction in the intensity) when the reaction environment became more oxidative. We believe this shift resulted from the formation of an ultrathin layer of silver oxide (Ag_2O) on the surface of each silver nanoparticle.[24] To further address this issue, we simulated the absorption spectra using the classical electrodynamic model developed for core–shell nanoparticles.[25] Because the dimensions of the silver nanoparticles are far smaller than the wavelength of illumination light, the absorption coefficient can be written as:[26]

$$Q = (4\pi r^3 n_0/3\lambda)[(\varepsilon_2 - \varepsilon_0)(\varepsilon_1 + 2\varepsilon_2) + f(\varepsilon_1 - \varepsilon_2)(\varepsilon_0 + 2\varepsilon_2)]/ [(\varepsilon_2 + 2\varepsilon_0)(\varepsilon_1 + 2\varepsilon_2) + f(2\varepsilon_2 - 2\varepsilon_0)(\varepsilon_1 - \varepsilon_2)] \quad (2)$$

Here r is the radius of the silver nanoparticles (assumed as spheres) covered by Ag_2O layers, n_0 is the refractive index of water, ε_0, ε_1, and ε_2 are relative permittivities of water, silver, and Ag_2O, respectively. The value f is the volume fraction occupied by the silver core: $f = (r_1/r)^3$, where r_1 is the radius of inner core of silver.

As shown in Fig. 5, there exists a strong dispersion in the

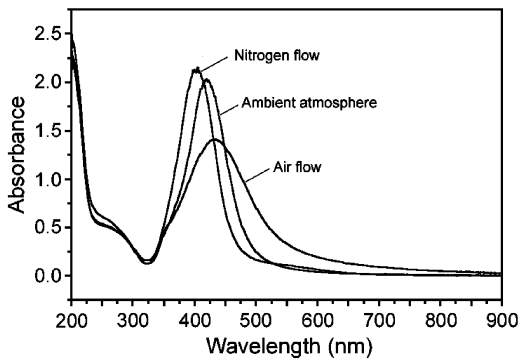

Fig. 4 The UV–Vis absorption spectra of three different samples of silver nanoparticles prepared at 27 °C under various environments: a continuous flow of nitrogen, ambient atmosphere, and a flow of air, respectively.

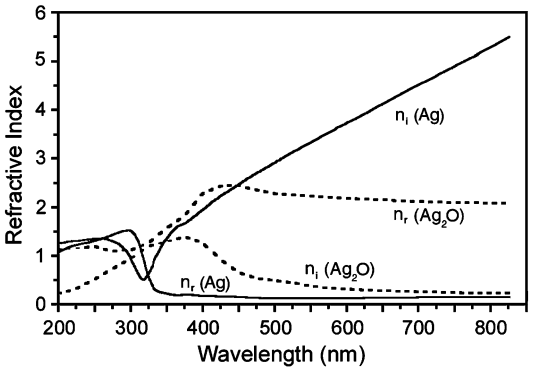

Fig. 5 Dispersion curves for the refractive indices of silver and silver oxide. The real and imaginary parts of the refractive index are labeled as n_i and n_r, respectively. The dielectric constant could be calculated from the refractive index by $\varepsilon = (n_r + in_i)^2$.

dielectric functions of silver and silver oxide.[27] To quantitatively determine the absorption coefficient of Ag–Ag_2O core–shell particles, we only used the experimentally measured values of the dielectric functions for these two materials as ε_1 and ε_2 in eqn. (2). The evolution of silver oxide was followed by comparing the absorption curves for core–shell nanoparticles with varying amounts of oxidation. In the simulation, we also assumed that the thickness of the Ag_2O film (Δr) is equivalent to the thickness of silver being oxidized (*i.e.*, $\Delta r = r - r_1$), with the initial radius of silver nanoparticles set at 20 nm. A plot of the absorption curves for four different oxidation levels (normalized as $\Delta r/r$) is shown in Fig. 6. As oxidation proceeded, the plasmon peak was reduced greatly in intensity, with its position red-shifted from 396 to 432 nm for oxidation levels up to 5.9%. Simultaneously, the width of the plasmon peak increased, and a small peak developed (at $\sim$360 nm) as the shoulder of the principal peak. Fig. 7 summarizes the dependence of the plasmon peak on the oxidation percentage. Both curves could be potentially employed to study the oxidation kinetics of silver nanoparticles.

The experimental results shown in Fig. 4 correlated well with the simulation studies. Under the nitrogen bubbling condition, the plasmon peak was centered at 398 nm, corresponding to silver nanoparticles of 20 nm in radius with no oxidation layers on their surfaces. This observation suggests that the nitrogen flow could effectively protect the silver surface from oxidation by the oxygen in air. As the fraction of oxygen in the surrounding environment increased, the plasmon peak continuously red-shifted from 398 nm through 417 nm under an atmosphere of air (without bubbling) to 431 nm under a constant flow of air. The peak intensity also decreased significantly by more than 30%, which was in agreement with the simulation results shown in Fig. 6. The oxidation of the surfaces of silver nanoparticles might also be responsible for

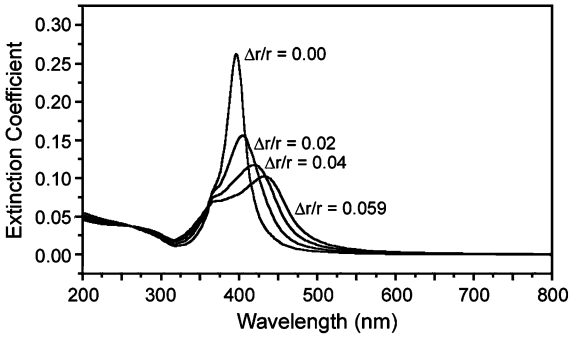

Fig. 6 The absorption coefficients of silver nanoparticles calculated for four different oxidation percentages, with $\Delta r/r$ being 0.0, 0.02, 0.04, and 0.059, respectively. Here Δr represents the thickness of silver oxide, and r the radius of silver nanoparticles before oxidation.

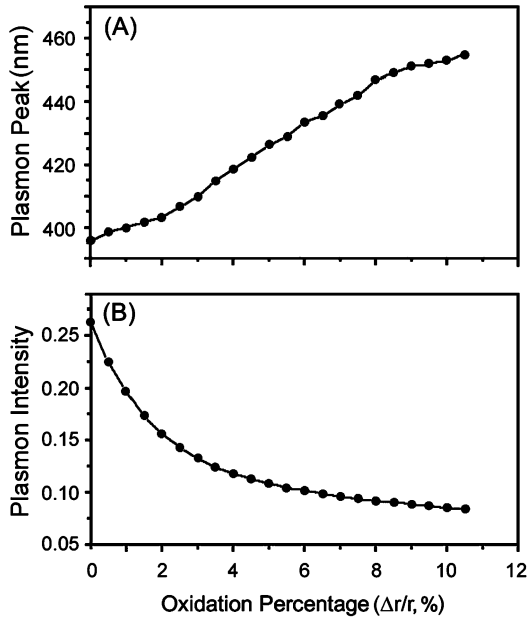

Fig. 7 A plot of the calculated position and intensity of the plasmon peak *versus* the oxidation percentage. Such a monotonous dependence could be employed to monitor the oxidation process (including kinetics) using the absorption spectroscopic method.

the broadening of the surface plasmon band, especially with the appearance of a shoulder peak around 350 nm: when the reaction was carried out under the protection of nitrogen gas, the experimental results showed no peak around 350 nm. In comparison, an obvious shoulder developed at this position when prepared under a flow of air. This observation is also consistent with the simulation results shown in Fig. 6.

Silver nanoparticles coated on microspheres

To further demonstrate the capability and versatility of this synthetic approach, silver nanoparticles were also prepared using a similar procedure as coatings on silica or polystyrene microspheres. Previous studies have indicated that such hybrid materials may have a range of applications in developing nonlinear optical devices, electrostatic shielding coatings, and supported catalysts.[28] When aqueous dispersions of silica or polystyrene microspheres were added to a mixture of diluted *SAB* and *SC* solutions, the silver nanoparticles were formed as decorative coatings on the surfaces of the microspheres, rather than as suspended objects in water. The microspheres coated with silver particles were collected by centrifugation and washed with deionized water. Fig. 8 shows the TEM image of a typical sample: 100 nm silica microspheres whose surfaces had

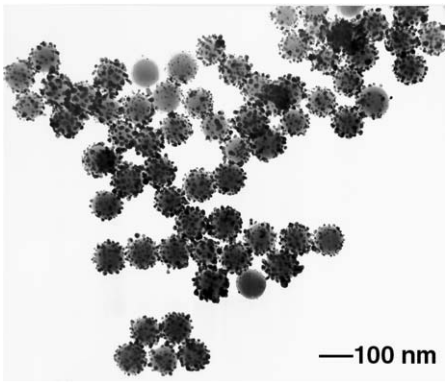

Fig. 8 TEM image of 100 nm silica beads whose surfaces had been coated with submonolayers of silver nanoparticles that were $\sim$20 nm in diameter.

been coated with silver nanoparticles. It can be clearly seen that the silver nanoparticles were homogeneously immobilized as discrete units on the surfaces of these silica bead. The size of the silver nanoparticles and their dispersion density on the surface of a microsphere could be easily controlled by changing the concentration of the silvering solutions.

IV. Conclusions

We have demonstrated a simple, convenient, and easy-to-control procedure for preparing silver nanoparticles with narrow size distributions in the range of 20–50 nm. These silver particles could be easily prepared either as stable aqueous dispersions or as decorative coatings on microspheres. The UV–Vis and TEM measurements indicate that the formation of these silver nanoparticles involved at least three distinctive stages: (1) nucleation, (2) growth and aggregation, and (3) Ostwald ripening of aggregates into discrete particles with a uniform size. Theoretical calculations were used to resolve the influence of surface oxidation on the absorption spectra of silver nanoparticles. We believe this method can be easily scaled up for the production of large volumes of silver nanoparticles since the reactants can be evenly mixed before precipitation takes place. As we have demonstrated, these aqueous dispersions of silver nanoparticles could be stored as long as for one year without observation of aggregates or sedimentation, which should make them particularly well-suited for industrial applications.

Acknowledgement

This work has been supported in part by a Career Award from the National Science Foundation (DMR-9983893), a Research Fellowship from the Alfred P. Sloan Foundation, and a Fellowship from the David and Lucile Packard Foundation. Y.Y. thanks the Center for Nanotechnology at the UW for a Graduate Fellowship Award. B.G. thanks the Center for Nanotechnology for an IGERT Fellowship Award funded by the NSF (DGE-9987620).

References

1 (*a*) G. Schmid and L. F. Chi, *Adv. Mater.*, 1998, **10**, 515; (*b*) J. H. Fendler and Y. Tian, *Nanopart. Nanostruct. Films*, 1998, 429; (*c*) W. P. Halperin, *Rev. Mod. Phys.*, 1986, **58**, 533.
2 (*a*) U. Kreibig and M. Vollmer, *Optical Properties of Metal Clusters*, Springer, Berlin, 1995; (*b*) M. A. El-Sayed, *Acc. Chem. Res.*, 2001, **34**, 257; (*c*) A. Henglein, *Chem. Rev.*, 1989, **89**, 1861; (*d*) M. Huang, A. Choudrey and P. Yang, *Chem. Commun.*, 2000, **12**, 1603.
3 J. Belloni, M. Mostafavi, J. L. Marignier and J. Amblard, *J. Imaging Sci.*, 1991, **35**, 68.
4 G. Schmid, *Clusters and Colloids: From Theory to Application*, VCH, Weinheim, 1994.
5 J. W. Slot and H. J. Geuze, *J. Cell Biol.*, 1983, **38**, 87.
6 (*a*) G. Carotenuto, G. P. Pepe and L. Nicolais, *Eur. Phys. J. B*, 2000, **16**, 11; (*b*) G. Carotenuto, *Appl. Organomet. Chem.*, 2001, **15**, 344.
7 R. J. Gehr and R. W. Boyd, *Chem. Mater.*, 1996, **8**, 1807.
8 (*a*) D. Fornasiero and F. Grieser, *J. Colloid Interface Sci.*, 1991, **141**, 168; (*b*) P. Matejka, B. Vlckova, J. Vohlidal, P. Pancoska and V. Baumrunk, *J. Phys. Chem.*, 1992, **96**, 1361.
9 (*a*) S. A. Nepijko, D. N. Levlev, S. Wilfried, J. Urban and G. Ertl, *Chem. Phys. Chem.*, 2000, **1**, 140; (*b*) A. Stabel, K. Eichhorst-Gerner, J. P. Rabe and A. R. GonzalezElipe, *Langmuir*, 1998, **14**, 7324.
10 (*a*) P-Y. Silvert, R. Herrera-Urbina, N. Duvauchelle, V. Vijayakrishnan and K. Tekaia-Elhsissen, *J. Mater. Chem.*, 1996, **6**, 573; (*b*) K. S. Chou and C. Y. Ren, *Mater. Chem. Phys.*, 2000, **64**, 241.
11 (*a*) A. Henglein, *Chem. Mater.*, 1998, **10**, 444; (*b*) M. Ji, X. Chen, C. M. Wai and J. L. Fulton, *J. Am. Chem. Soc.*, 1999, **121**, 2631; (*c*) S. Pethkar, M. Aslam, I. S. Mulla, P. Ganeshan and K. Vijayakrishnan, *J. Mater. Chem.*, 2001, **11**, 1710; (*d*) R. A. Salkar, P. Jeevanandam, S. T. Aruna, Y. Koltypin and A. Gedanken, *J. Mater. Chem.*, 1999, **9**, 1333.
12 (*a*) M. Okumura, S. Tsubota, M. Iwamoto and M. Haruta, *Chem. Lett.*, 1998, **4**, 315; (*b*) N. Keeda and G. L. Messing, *J. Mater. Res.*, 1998, **13**, 1660.
13 (*a*) N. Yanagihara, K. Uchida, M. Wakabayashi, Y. Uetake and T. Hara, *Langmuir*, 1999, **15**, 3038; (*b*) L. Armelao, R. Bertoncello and M. De Dominicis, *Adv. Mater.*, 1997, **9**, 736; (*c*) G. De, A. Licciulli, C. Massaro, L. Tapfer, M. Catalano, G. Battaglin, C. Meneghini and P. Mazzoldi, *J. Non-Cryst. Solids*, 1996, **194**, 225.
14 (*a*) J. A. Creighton and D. G. Eadon, *J. Chem. Soc., Faraday Trans.*, 1991, **87**, 3881; (*b*) P. J. Hull, J. L. Hutchison, O. V. Salata and P. J. Dobson, *Adv. Mater.*, 1997, **9**, 413.
15 (*a*) C. D. Sanguesa, R. H. Urbina and M. Figlar, *J. Solid State Chem.*, 1992, **100**, 272; (*b*) D. Burshtain, L. Zeiri and S. Efrima, *Langmuir*, 1999, **15**, 3050; (*c*) Y.-S. Shon, R. Colorado Jr., C. T. Williams, C. D. Bain and T. R. Lee, *Langmuir*, 2000, **16**, 541.
16 See, for example: (*a*) I. Pastoriza-Santos and L. M. Liz-Marzan, *Langmuir*, 1999, **15**, 948; (*b*) W. Wang, X. Chen and S. Efrima, *J. Phys. Chem. B*, 1999, **103**, 7238; (*c*) P.-Y. Silvert, R. Herrera-Urbina, N. Duvauchelle, V. Vijayakrishnan and K. T. Elhsissen, *J. Mater. Chem.*, 1996, **6**, 573; (*d*) L. O. Brown and J. E. Hutchison, *J. Am. Chem. Soc.*, 1999, **121**, 882.
17 A. G. Ingalls, *Amateur Telescope Making (Book One)*, Scientific American Inc., New York, 1981, p. 101.
18 For example, Peacock Laboratories, Inc. Philadelphia, PA, 19143.
19 D. L. V. Hyning and C. F. Zukoski, *Langmuir*, 1998, **14**, 7034.
20 (*a*) K. S. Suslick, T. Hyeon and M. Fang, *Chem. Mater.*, 1996, **8**, 2172; (*b*) M. M. Mdleleni, T. Hyeon and K. S. Suslick, *J. Am. Chem. Soc.*, 1998, **120**, 6189; (*c*) A. Kornath and F. Neumann, *Inorg. Chem.*, 1997, **36**, 2708; (*d*) F. D. Smet and M. Devillers, *Chem. Mater.*, 1999, **11**, 324.
21 S. M. Heard, F. Grieser, C. G. Barraclough and J. Sanders, *J. Colloid Interface Sci.*, 1983, **93**, 545.
22 (*a*) S. Biggs, M. K. Chow, C. F. Zukoski and F. Grieser, *J. Colloid Interface Sci.*, 1993, **160**, 511; (*b*) M. K. Chow and C. F. Zukoski, *J. Colloid Interface Sci.*, 1994, **165**, 97.
23 D. L. Van Hyning, W. C. Klemperer and C. F. Zukoski, *Langmuir*, 2001, **17**, 3120.
24 S. Kapoor, *Langmuir*, 1998, **14**, 1021.
25 C. F. Bohren and D. R. Huffman, *Absorption and Scattering of Light by Small Particles*, Wiley, New York, 1983.
26 (*a*) U. Kreibig, M. Gartz and A. Hilger, *Ber. Bunsen-Ges. Phys. Chem.*, 1997, **101**, 1593; (*b*) P. Mulvaney, *Langmuir*, 1996, **12**, 788.
27 L. A. A. Pettersson and P. G. Snyder, *Thin Solid Films*, 1995, **270**, 69.
28 (*a*) J. Y. Bigot, J. C. Merle, O. Cregut and A. Daunois, *Phys. Rev. Lett.*, 1995, **75**, 4702; (*b*) Z. Qi and P. G. Pickup, *Chem. Commun.*, 1997, 1008; (*c*) C. W. Chen, M. Q. Chen, T. Serizawa and M. Akashi, *Adv. Mater.*, 1998, **10**, 1122; (*d*) Y. Kobayashi, V. Salgueiriño-Maceira and L. M. Liz-Marzán, *Chem. Mater.*, 2001, **13**, 1630.